CILAMCE 2017
Florianópolis - Santa Catarina - Brazil

ASSESSMENT OF THE SENSITIVITY OF THE WRF MODEL USING DIFFERENT PBL SCHEMES OVER THE METROPOLITAN REGION OF SALVADOR

Yasmin Kaore Lago Kitagawa[1]

ykaore@gmail.com

Erick Giovani Sperandio Nascimento[2]

Noéle Bissoli Perini de Souza[1]

Georgynio Yossimar Rosales Aylas[2]

Pedro Junior Zucatelli[1]

Nadir Salvador[1]

Davidson Martins Moreira[2]

[1]Federal University of Espírito Santo (UFES)

Avenue Fernando Ferrari, 514 - Goiabeiras, 29075-910, Vitória, Espírito Santo, Brazil

[2]Centro Integrado de Manufatura e Tecnologia (SENAI CIMATEC)

Avenue Orlando Gomes, 1845 - Piatã, 41650-010, Salvador, Bahia, Brazil

Abstract. *Sensitivity of the Weather Research Forecasting (WRF) model has been carried out using six planetary boundary layer (PBL) schemes – Bougeault-Lacarrere (BouLac), Grenier-Bretherton (GBM), Mellor-Yamada-Janjić (MYJ), Mellor-Yamada-Nakanishi-Niino (MYNN), Bretherton-Park (UW) and Yonsei University (YSU) - over the Metropolitan Region of Salvador (RMS) for surface meteorological parameters and PBH height (PBLH) during wet (AMJJ) and dry (SOND) period. The aim is to evaluate the performance of these parameterizations, selecting the best option for the RMS for the purpose of contribute with scientific background on the local atmospheric circulation, air pollution problems and researches related to eolic and solar energy in the region. The model outputs have been compared with observations through statistical measures – mean bias (MB), root mean square error (RMSE), correlation coefficient (r) and index of agreement (IOA). Overall, MYJ shows the best performance for temperature, wind speed and direction, whereas UW and MYNN also show good agreement for wind direction during wet and dry period, respectively. The PBLH was not compared against observations, since they are not available. However, it was noticed that BouLac simulated deepest PBLH, whereas UW and GBM simulated shallowest PBLH for both periods. Considering all, it is seen that MYJ scheme works reasonably well for RMS.*

Keywords: *planetary boundary layer, WRF model, atmospheric modeling, Bahia.*

1 INTRODUCTION

Numerical weather prediction (NWP) models take the equations of fluid mechanics and thermodynamics to describe the atmospheric processes. NWP have become an important tool for weather forecasting and other various applications dependent on meteorological information, such as: air pollution researches and, assessment of wind and solar power production over a region.

Part of the research efforts in meteorology are concentrated on the lowest part of the troposphere, commonly known as the Planetary Boundary Layer (PBL) that is directly influenced by the presence of the Earth's surface (Stull, 1988). Exchanges of moisture, heat, and momentum occur within the PBL through mixing associated with turbulent eddies. These eddies influence the way in which lower-tropospheric thermodynamic and kinematic structures evolve. However, such eddies operate on spatiotemporal scales that cannot be explicitly represented on grid scales and time steps employed in most mesoscale models. As such, their effects are expressed in these models via the use of PBL parameterization schemes, which use physical assumptions and empirical approximations to represent the physical processes.

Proper description of the physical processes related to the PBL is one of the most challenging tasks in mesoscale numerical simulation and prediction. The mesoscale model used in this work is the Weather Research and Forecasting (WRF) model version 3.9. The WRF is a mesoscale numerical weather prediction model used for atmospheric researches and operational applications. Its physical parameterizations can be divided into different categories, each one containing multiple available options of PBL, land surface, surface layer, microphysics, cumulus parameterization and radiation (longwave and shortwave).

The accurate of the modelling results are strongly depending upon the ability of the numerical models to correctly represent and simulate the PBL processes (Carvalho et al., 2014; Boadh et al., 2016). In this way, several studies have been developed to evaluate the performance of WRF model to different PBL schemes. However, the study of these schemes is not trivial and requires several simulations and, consequently, computational resources. Besides, the PBL parameterizations in numerical models have been mostly tested in subtropical and higher latitudes and very few studies (Srinivas et al., 2007b; Sanjay, 2008) exist over tropical regions or lower latitudes (Hariprasad et al., 2014; Surussavadee, 2017).

Therefore, this study aims to evaluate the performance of six PBL parameterization schemes – Bougeault and Lacarrere (BouLac), Grenier and Bretherton (GBM), Mellor-Yamada-Janjić (MYJ), Mellor-Yamada-Nakanishi-Niino 2.5(MYNN), Bretherton and Park (UW) and Yonsei University (YSU) – using the WRF model, over the Metropolitan Region of Salvador (RMS), in order to provide some scientific background on the local atmospheric circulation (for example, air pollution problems and researches related to eolic and solar energy in the region) during the wet (April-May-June-July) and dry (September-October-November-December) period based on surface meteorological parameters, namely 2-meter Temperature (T2), 10-meter wind Speed (WS10) and 10-meter wind direction (WD10).

It is interesting to point out that the Brazilian northeast has been receiving a gradually increasing amount of investment in several sectors, including the energy sector. According to the Ministry of Mines and Energy of Brazil, this region has very favorable wind conditions and, because of that, it presents the country's largest installed capacity for solar and wind farms. However, the lack of studies and reliable information can represent a drawback for the economic development of the region.

Notwithstanding the growing industrialization and urbanization can lead to potential transformations in the environmental conditions, justifying the choice of this region. Besides, the fact that there is no previous work performing any assessment in this area using WRF model which is the motivation of this study.

2 METHODOLOGY AND DATA

2.1 Study area

The RMS is an urban-industrial area with a peninsular configuration, where the "Todos os Santos" bay is located in the south-west of the region and, the Atlantic Ocean in the east (Figure 1).

The RMS is formed by thirteen cities and it is occupied by 3.6 million habitants distributed over an area of 4 375 km^2 (IBGE, 2010). The cities include: Camaçari, Candeias, Dias d'Ávila, Itaparica, Lauro de Freitas, Madre de Deus, Mata de São João, Pojuca, Salvador, São Francisco do Conde, São Sebastião do Passé, Simões Filho and Vera Cruz; being Salvador (13º01'S, 38º31'W) the major city and also the capital of the state of Bahia.

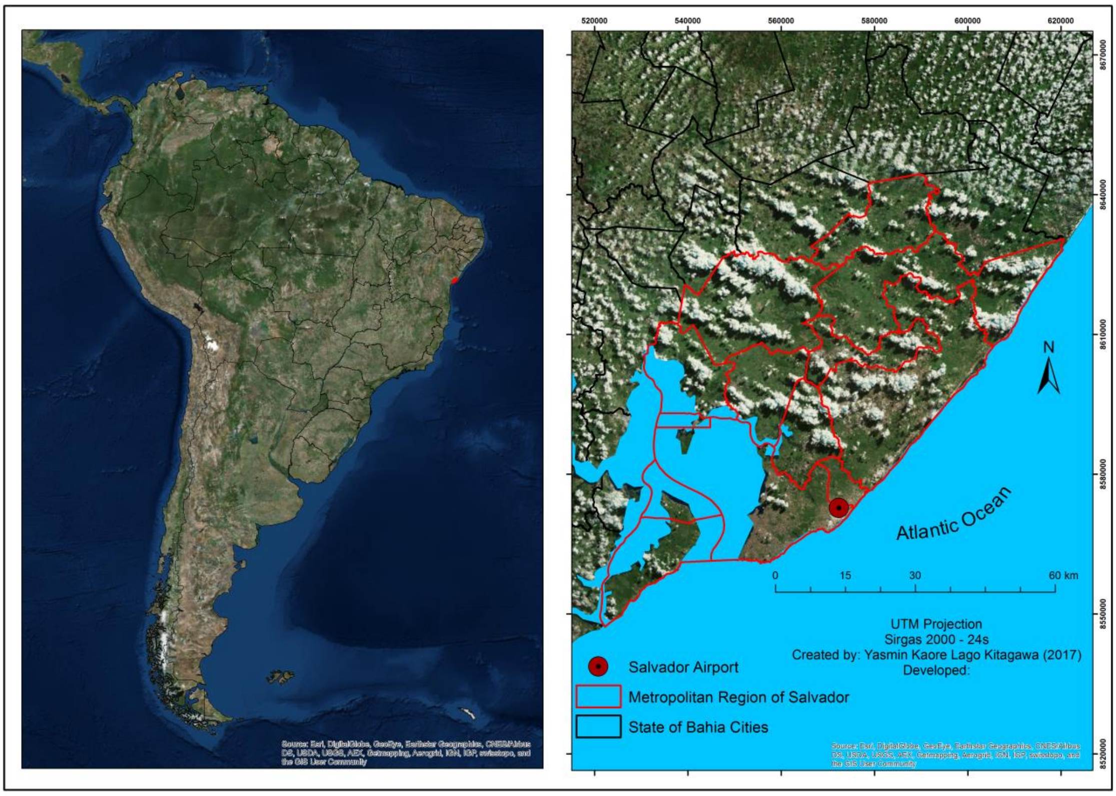

Figure 1: The location of the RMS in Brazil (left) and in Bahia State (right).

According to the Köppen climate classification, Bahia's coastline is located within the tropical humid climate that constitutes the so-called "Af zone", with occurrences of precipitation monthly and the lack of a defined dry season. Even so, Rao et al. (1993), Barreto et al. (2008) and Santos (2013) analyzed the rainfall index of the city of Salvador and identified the wet period as April-May-June-July (AMJJ) whereas the less rainy period is

September-October-November-December (SOND). According to Queiroz (2015), several atmospheric systems act on the Northeast Region and affect, directly or indirectly, the rainfall regime of Salvador, namely: Intertropical Convergence Zone (ZCIT), South Atlantic Subtropical Anticyclone (ASAS), South Atlantic Convergence Zone (ZCAS), Easterly Wave Disturbances (DOL), Front Systems (SF), High Level Cyclonic Vortices (VCAN), Mesoscale Convective System (SCM) and Sea Breeze Systems.

The average annual temperature in Salvador is 25.7°C, and monthly averages vary between 23.7°C in August and 27.1°C in February and March. Relative humidity is high throughout the year, with an annual average of about 80%, where February is less humid (79.2%) and May is the most humid (83.9%), reaching a maximum humidity of 94.6%.

Silva (2014) analyzed the wind speed and direction between 2003 and 2011 and, showed that the predominance of wind direction in the RMS during the year is from the east, followed by the east-southeast direction. The east (E) wind remains predominant between the months of October to March. The south (S) and east-southeast (ESE) wind are predominant in June and July while the south (S) and southeast (SE) wind are predominant in May and August. The author also suggested that the months of April and September are transitional.

In terms of the hourly average wind speed, the highest values occur in the afternoon and, the lowest ones during the dawn and the early hours of the morning. The maximum daily amplitude of wind speed occurs in the months of November and December, and the minimum in June and July.

2.2 Model description

The NWP model used in this work to perform the meteorological parameters simulations was the Weather and Research Forecast (WRF) model. The model was developed by the National Centre for Atmospheric Research (NCAR) and others American agencies.

The WRF system contains two dynamical solvers, referred to as the ARW (Advanced Research WRF) core and the NMM (Nonhydrostatic Mesoscale Model) core. ARW dynamical solver was the one used in this work. The WRF-ARW core integrates the fully compressible nonhydrostatic Euler equations, with terrain-following hydrostatic pressure vertical coordinates.

The prognostic variables include three dimensional wind, perturbation quantities of potential temperature, geopotential and surface pressure of dry air, turbulent kinetic energy and scalars (water vapor, rain/snow, cloud water/ice mixing ratio, etc.).

The grid format in the horizontal plane is Arakawa-C and time integration is performed with a 2^{nd} and 3^{rd}-order Runge-Kutta scheme with a smaller time step for acoustic and gravity-wave modes. The spatial discretization, in both horizontal and vertical directions, uses 2^{nd} to 6^{th}-order advection schemes. Detailed information about the physics, equations and dynamics can be found on Skamarock et al. (2008).

2.3 WRF-ARW physical parameterizations

WRF presents different physics schemes for the sake of representing the sub-grid processes effects in the simulation grid. Sub-grid processes are usually described as physical processes that happen at a spatial and/or temporal scale smaller than the model grid/time step resolution. In order to get these sub-grid processes effects, physical parameterization schemes are employed which include: microphysics, cumulus parameterization, surface layer and land surface parameterization, PBL, longwave and shortwave radiation.

Microphysics parameterization embraces explicitly resolved water vapor, cloud and precipitation processes. At the end of each time step, a saturation adjustment is made in favor of the updated of temperature and humidity. Cumulus parameterization is responsible for sub-grid effects of convective and/or shallow clouds, providing also vertical distribution of moisture and heat. Surface layer schemes calculate friction velocities and exchange coefficients used in the calculation of surface heat and moisture fluxes by the land-surface models (LSM) and surface stress in the PBL schemes. The LSMs provide heat and moisture fluxes over land and sea-ice points through combining different information from the surface layer, radiation and microphysics schemes, and also from land's state variables and land-surface properties. PBL schemes are responsible for representing the vertical sub-grid scale fluxes due to turbulent mixing throughout the entire grid column, not just in the boundary layer. The radiation schemes provide the atmospheric heating due to radiative flux divergence and surface downward longwave and shortwave radiation for the ground heat budget (Skamarock et al., 2008). In this work, we focus on the PBL parameterization schemes.

2.4 WRF PBL schemes

The treatment of exchange processes of moisture, heat, and momentum into the PBL by the WRF model takes account two major components: the order of turbulence closure and whether a local or a nonlocal mixing approach is employed.

In the set of equations for turbulent flow, the number of unknowns is larger than the number of equations, and this is known as the turbulence closure problem. The unknown term is always of one order above the maximum among the other terms. Because of this, turbulence closure requires empirically relating the unknown term of moment n+1 to lower-moment known terms. The PBL schemes in the WRF model can be one or one-and-half order closure. In addition to that, whether the fluxes are determined from known local variables, it is so-called local closure. In this treatment, only those vertical levels that are directly adjacent to a given point directly affect variables at the given point. In case of non-local closure, as the name said, non-local fluxes are added, and then multiple vertical levels can be used to determine a variable at a given point (Hu et al., 2010; Xie et al., 2012; Cohen et al., 2015; Gunwani & Mohan, 2017). Among the six PBL schemes that will be evaluated in this study, the BouLac, GBM, MYJ, MYNN and UW scheme are local closure models, while the YSU scheme is a nonlocal model. An overview of the PBL schemes selected for this study is shown below.

YSU scheme is a first order and non-local scheme which uses non-local eddy diffusivity coefficients to compute turbulent fluxes, and treats the entrainment layer, at the top of the PBL, explicitly. The non-local vertical fluxes are reached by adding a non-local gradient adjustment term (the countergradient term – γ_c) to the local gradient for any prognostic variables ($C, u, v, \theta, q, q_c, q_i$) (Hong et al., 2006):

$$\frac{\partial C}{\partial t} = \frac{\partial}{\partial z}\left[K_c\left(\frac{\partial C}{\partial z} - \gamma_c\right) - \overline{(v'w')}_h\left(\frac{z}{h}\right)^3\right] \tag{1}$$

Where K_c is the eddy diffusivity coefficient, γ_c is a correction to the local gradient that considers the large scale eddies to the total flux, $\overline{(v'w')}_h$ is the flux at the inversion layer and h is the PBL height.

The non-local closure scheme calculates the PBL height using the Richardson bulk number method from some predetermined starting level (Banks et al., 2016; Salvador et al., 2016), in the case of YSU, the critical Richardson number (R_i) for the entire PBL is 0.25. For the MYJ (Janjic, 1994), MYNN (Nakanishi & Niino, 2006), BouLac (Bougeault & Lacarrere, 1989), GBM (Grenier & Bretherton, 2001) and UW (Bretherton & Park, 2009) PBL schemes, which are 1.5 order turbulent local closure models, the PBL height is determined at a level where the turbulent kinetic energy (TKE) profile decreases to some predefined threshold value.

2.5 Model simulation details

The study was carried out using the Weather Research and Forecasting (WRF) model version 3.9 with the ARW dynamical solver.

The WRF meteorological input data came from National Centers for Environmental Prediction (NCEP) Final Analysis (FNL) on 0.25º x 0.25º grids resolution at every six hours. The land use data were provided by United States Geological Survey (USGS) at 5 min, 2 min and 30 s resolutions.

The WRF-ARW simulations were carried out monthly, including 24h for spin-up in order to obtain realistic initial conditions, in other words, each month's simulation was initialized from 00:00 UTC of the last day of the previous month.

The model was run with three nested domains with grid resolutions of 9 km, 3 km and 1 km, respectively. An overview of the spatial configurations is shown in Table 1. The domain of interest has horizontal resolution of 1 km and twenty-three vertical levels with the model top set at 50 hPa.

The others physics options adopted (Table 2) and, left unchanged for all the runs, were: WRF single-moment 5-class microphysics (Hong et al., 2004), Kain-Fritsch cumulus parametrization (Kain, 2004), Dudhia shortwave radiation (Dudhia, 1989), Rapid Radiative Transfer Model (RRTM) longwave radiation (Mlawer et al., 1997), and the Noah land-surface model. In the second and third domain which was run at 3 km and 1km spatial resolution, respectively, simulations were carried out using explicit convection.

Table 1. Details of the model configuration.

Simulation	D01	D02	D03
Horizontal resolution	9 km	3 km	1 km
Domains of interest	11.18°-14.33° S 36.68º-39.92º W	11.99°-13.61° S 37.59º-39.25º W	12.18°-13.37° S 37.78º-39.00º W
Grid size	39x39	60x60	132x132
Resolution	351 km	180 km	132 km
Vertical resolution		23 sigma levels	

Table 2. Simulation details specifying physics options.

Simulation	1	2	3	4	5	6
Surface layer	MM5	MM5	Eta	MYNN	MM5	MM5
PBL	BouLac	GBM	MYJ	MYNN	UW	YSU
Microphysics	WSM5-class scheme					
Cumulus	Kain-Fritsch scheme					
Shortwave radiation	Dudhia scheme					
Longwave radiation	RRTM scheme					
Land surface model	Noah land surface scheme					

2.6 Statistical metrics

For validating the ARW model simulations, available meteorological observations of T2, WS10 and WD10 from the Salvador Airport (12.91°S, 38.33ºW) were used. The location of the surface meteorological station is shown in Figure 1.

The model performance was evaluated using statistical measures of bias, root mean square error (RMSE), correlation coefficient (r) and index of agreement (IOA) (Hariprasad et al., 2014; Carvalho et al., 2014; Banks et al., 2016; Boadh et al., 2016; Gunwani & Mohan, 2017; Surussavadee, 2017). The mean error, also referred to as bias, is given by the relation 2:

$$Bias = \bar{M} - \bar{O} \qquad (2)$$

If the biases present positives values, it indicates that the model overestimates the values while negatives biases imply that model underestimates the values.

The RMSE expresses the total model error and its value is zero for ideal cases:

$$RMSE = \sqrt{\frac{1}{n}\sum_{i=1}^{n}(M_i - O_i)^2} \qquad (3)$$

For both cases, smaller values indicate better agreement between observed and modeled data.

Correlation coefficient (r) is a measure of the linear association between the modeled and observed data, with zero indicating the absence of correlation:

$$r = \frac{\sum_{i=1}^{n}[(M_i - \bar{M})(O_i - \bar{O})]}{\sqrt{\sum_{i=1}^{n}(M_i - \bar{M})^2 \sum_{i=1}^{n}(O_i - \bar{O})^2}} \qquad (4)$$

The IOA was developed by Willmott (1981) as a standardized measure of the degree of model prediction error and varies between 0 and 1:

$$IOA = 1 - \left[\frac{\sum_{i=1}^{n}(M_i - O_i)^2}{\sum_{i=1}^{n}(|M_i - \bar{O}| + |O_i - \bar{O}|)^2}\right] \qquad (5)$$

A value of 1 indicates a perfect match, and 0 indicates no agreement at all. M_i represents the modeled data, O_i represents the observed data, $\bar{M}$ represents the modeled mean, $\bar{O}$ represents the observed mean and *n* is the total number of observations.

Emery et al. (2001) suggested statistical benchmarks for the meteorological parameters, for wind speed: bias ± 0.5 m/s, RMSE < 2.0 m/s and IOA > 0.6. For temperature, bias ± 0.5 K and IOA > 0.8, and for wind direction bias ± 10º.

3 RESULTS AND DISCUSSION

3.1 Diurnal evolution and statistical analysis of the surface parameters

The time variations of the surface level meteorological variables simulated by WRF-ARW at Airport station along with observations in April (a), May (b), June (c), July (d), September (e), October (f), November (g) and December (h) are presented in Figures 2–4. As can be seen, the model was able to capture the evolution of the diurnal variation.

Figure 2 shows the mean diurnal variation of T2 for wet and dry seasons. Most PBL schemes underestimate T2 during daytime in both periods, except for MYJ that overestimates T2 during daytime in dry period. Overall, by analyzing Figure 2, during daytime, for wet season, MYJ scheme shows a better agreement with observations whereas for dry season, MYNN together with MYJ appear with better concordance.

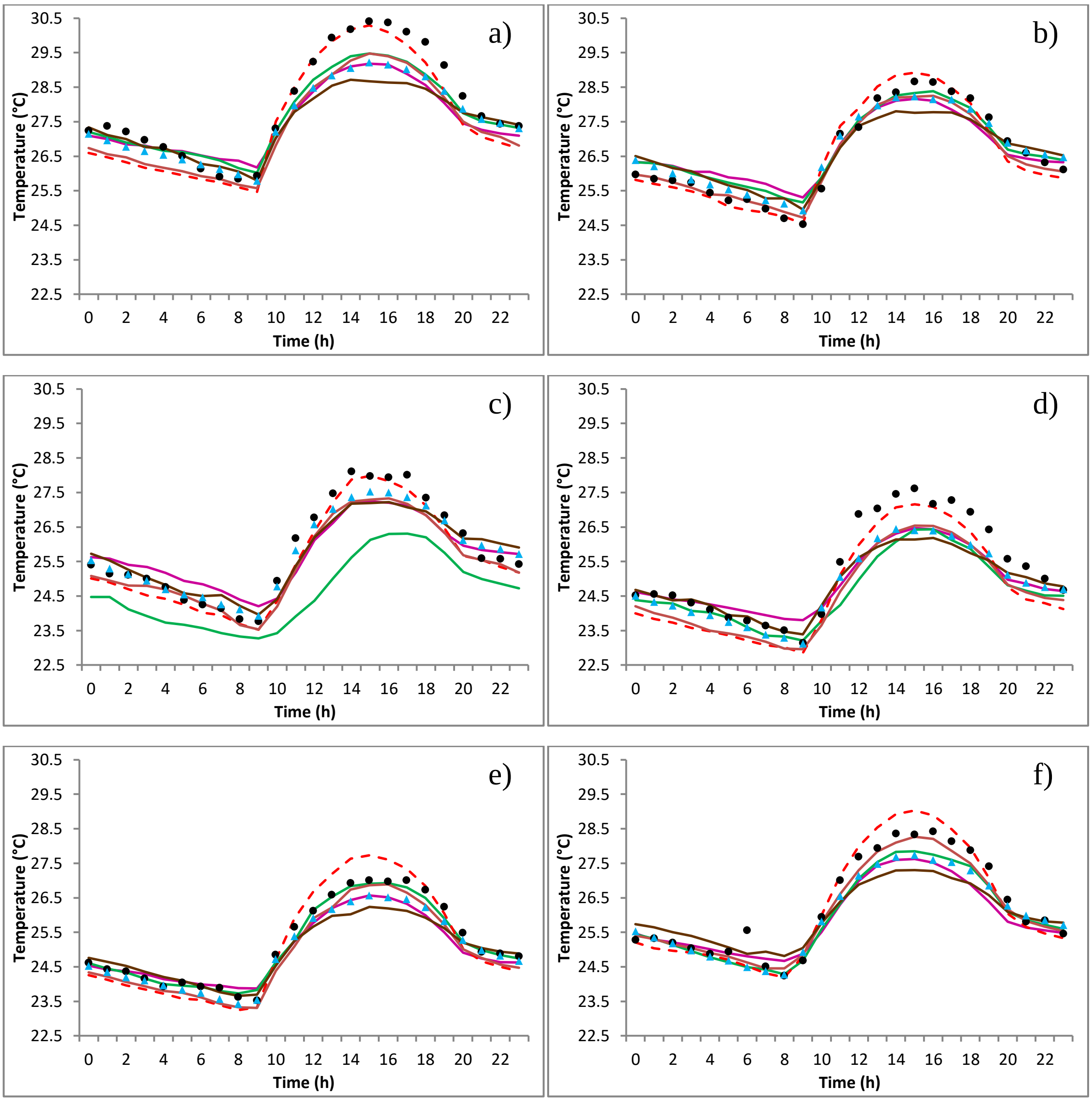

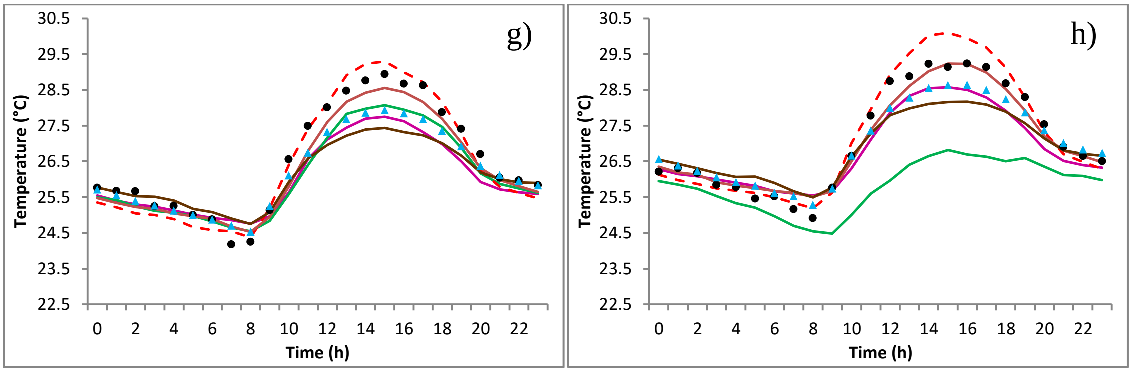

Figure 2: Time variation of T2 for wet period (AMJJ) and dry period (SOND).

• Observation — BouLac — GBM - - - MYJ
— MYNN — UW ▲ YSU

Table 3 shows wet and dry statistics for T2 separated monthly. All simulations present high index of agreement (IOA>0.8 or close to that), except for GBM in June and December. Bias also lie on in acceptable range (Bias<±0.5 K), except for GBM again in June and December. All simulations, in both periods, underestimate the T2 values; with exception of May which is the only month that overestimated the values of T2 (excluding the simulations MYJ and MYNN).

One can see that MYJ scheme is much highlighted in Table 3 than the others, meaning that overall it is the PBL scheme with better agreement for the depiction of T2.

Table 3. Statistics of the comparison between observed and simulated T2 data.

Month	Statistics	BouLac	GBM	MYJ	MYNN	UW	YSU
April	Bias	-0.45	**-0.30**	-0.41	-0.63	-0.52	-0.44
	RMSE	1.18	**1.08**	**1.08**	1.16	1.31	1.15
	R	0.82	0.83	**0.84**	**0.84**	0.75	0.81
	IOA	0.83	0.86	**0.90**	0.86	0.78	0.85
May	Bias	0.10	0.14	-0.03	-0.12	**0.02**	0.10
	RMSE	1.37	1.39	1.38	**1.34**	1.36	1.35
	R	0.67	0.65	**0.68**	**0.68**	**0.68**	**0.68**
	IOA	0.75	0.77	**0.82**	0.79	0.76	0.78
June	Bias	-0.11	-1.23	-0.30	-0.39	-0.13	**-0.08**
	RMSE	1.25	2.74	1.22	1.24	1.24	**1.13**
	R	0.75	0.27	0.77	0.78	0.75	**0.80**
	IOA	0.82	0.53	**0.87**	0.85	0.84	**0.87**
July	Bias	**-0.34**	-0.62	-0.55	-0.68	-0.41	-0.46
	RMSE	1.26	1.55	1.24	1.27	1.24	**1.22**
	R	0.76	0.66	0.80	**0.81**	0.78	0.79
	IOA	0.80	0.78	**0.86**	0.84	0.82	0.83

September	Bias	-0.21	-0.07	**-0.05**	-0.30	-0.22	-0.23
	RMSE	1.00	0.99	1.09	1.00	1.06	**0.95**
	R	0.77	0.76	0.76	0.78	0.73	**0.79**
	IOA	0.83	0.86	**0.87**	**0.87**	0.80	0.86
October	Bias	-0.34	-0.29	**-0.01**	-0.15	-0.24	-0.26
	RMSE	1.49	1.47	1.40	**1.38**	1.53	1.45
	R	0.68	0.67	**0.71**	**0.71**	0.64	0.68
	IOA	0.73	0.77	**0.83**	0.80	0.69	0.77
November	Bias	-0.49	-0.40	**-0.07**	-0.23	-0.41	-0.30
	RMSE	1.19	1.40	**1.02**	1.05	1.26	1.09
	R	0.82	0.80	**0.91**	0.89	0.78	0.86
	IOA	0.80	0.67	**0.83**	0.81	0.75	0.82
December	Bias	-0.28	-1.28	0.16	**-0.05**	-0.21	-0.11
	RMSE	0.97	2.29	0.90	**0.86**	1.00	0.90
	R	0.84	0.33	**0.87**	0.86	0.84	0.85
	IOA	0.87	0.56	**0.93**	0.91	0.85	0.89

The time variation of WS10 (Figure 3) depicts the increase of the wind speed between 9-10 h until around 16 h, when the wind speed values start to decay.

In the early hours of the morning, MYJ and YSU schemes seem to show a better concordance with observations for both periods; GBM also appears to be very similar with MYJ in the wet period during the early hours of the morning. However, by evaluating the next hours, one can say that during the wet period (Figure 3a-d), UW follows the same tendency of MYJ (sometimes better than MYJ), nevertheless, in the beginning of the evening; UW does not capture very well the change in the wind speed values. UW follows the same tendency of MYJ (sometimes better than MYJ), nevertheless, in the beginning of the evening; UW does not capture very well the change in the wind speed values. By considering daytime in the dry period (Figure 3e-h), all PBL schemes overestimate the WS10 values, presenting the biggest discrepancies when compared at the same time in the wet period.

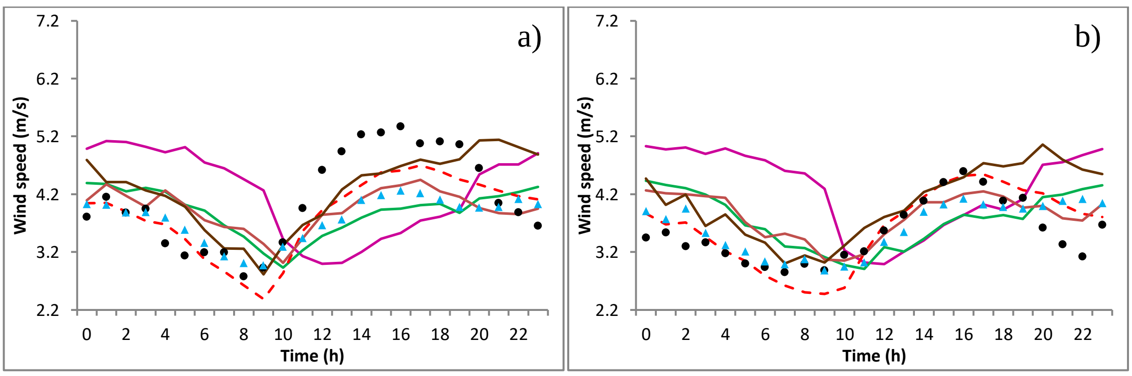

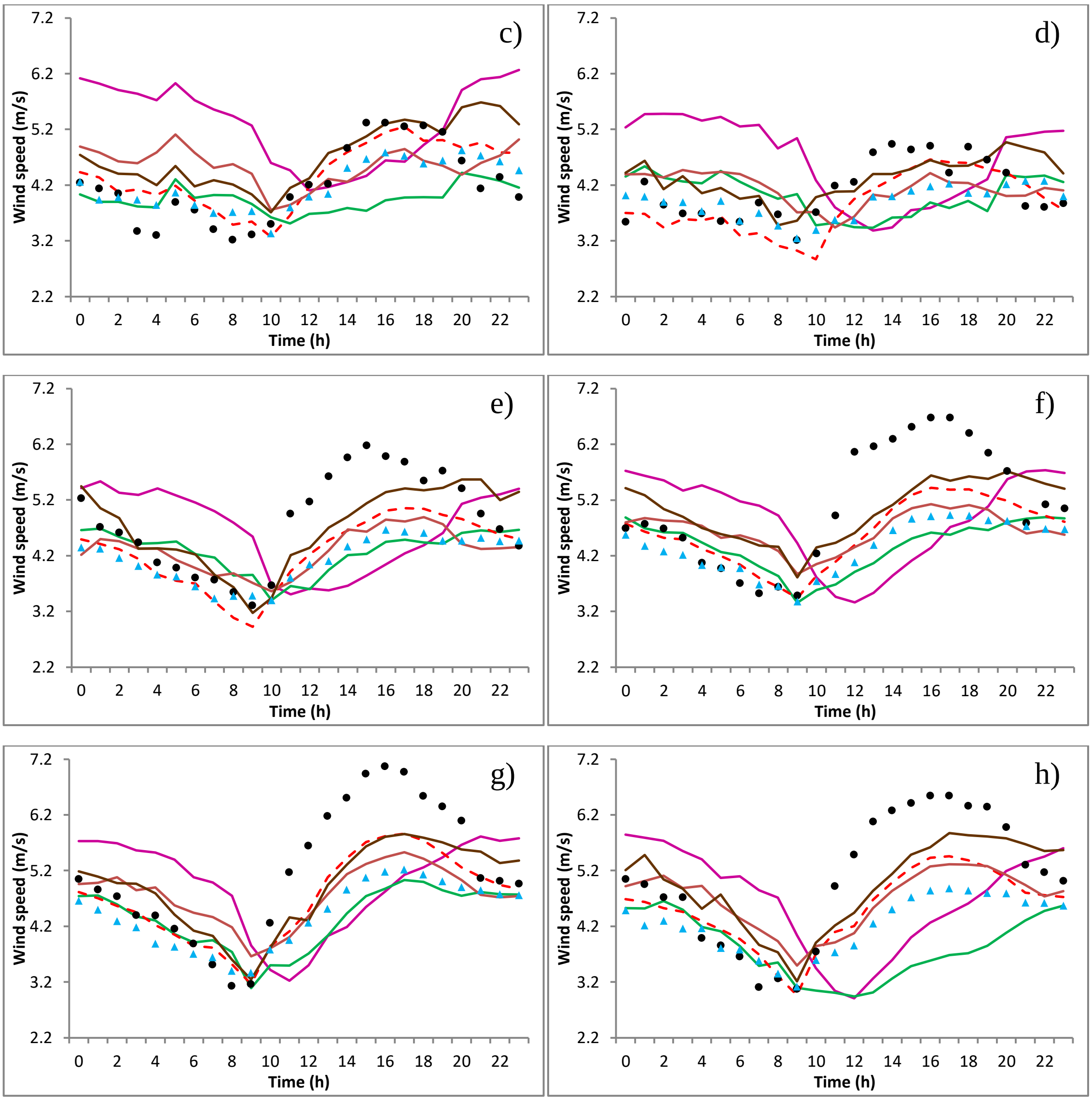

Figure 3: Time variation of WS10 for wet period (AMJJ) and dry period (SOND).

Observation BouLac GBM MYJ
MYNN UW YSU

Table 4 shows the statistical metrics for WS10 separated monthly. All simulations present high index of agreement (IOA>0.6), except for BouLac and GBM in May, September, October and December. It is noticeable that predominantly during dry season, namely BouLac and GBM, IOA are the lowest. Bias and RMSE also are in acceptable range for both periods (Bias<±0.5 m/s; RMSE<2 m/s) since the values are within these ranges or very close to it. It is worth mentioning that during dry period any of YSU simulations present Bias<0.5, proposed by Emery. Even Figures 3e-f are showing overprediction of WS10 during the daytime, by analyzing the Table 4, it can be seen that all PBL schemes underestimate WS10 during dry season; while during wet period some of them are under-predicted and others are over-predicted. May is the only month again which present all simulations overestimated. Once again, it is evident that MYJ presents the best statistical scores (RMSE, r, IOA) for both periods, despite YSU shows the lowest Bias during wet season and UW during dry season.

Table 4. Statistics of the comparison between observed and simulated WS10 data.

Month	Statistics	BouLac	GBM	MYJ	MYNN	UW	YSU
April	Bias	**0.11**	-0.21	-0.26	-0.16	0.15	-0.33
	RMSE	1.84	1.48	**1.24**	1.40	1.49	1.32
	r	0.06	0.33	**0.60**	0.42	0.42	0.52
	IOA	0.39	0.54	**0.74**	0.61	0.65	0.62
May	Bias	0.74	0.22	0.10	0.30	0.52	**0.09**
	RMSE	1.94	1.50	1.44	1.44	1.61	**1.40**
	r	0.40	0.51	**0.57**	0.56	0.54	0.56
	IOA	0.63	0.70	**0.75**	0.72	0.72	0.71
June	Bias	1.08	-0.27	0.18	0.33	0.54	**-0.01**
	RMSE	2.45	1.92	1.61	1.76	1.88	**1.50**
	r	0.54	0.58	**0.67**	0.61	0.63	0.65
	IOA	0.68	0.76	**0.82**	0.77	0.78	0.80
July	Bias	0.55	-0.09	-0.24	**0.03**	0.22	-0.21
	RMSE	1.81	1.40	**1.22**	1.33	1.45	**1.22**
	r	0.53	0.61	**0.73**	0.66	0.63	0.69
	IOA	0.71	0.78	**0.85**	0.81	0.79	0.80
September	Bias	-0.15	-0.54	-0.55	-0.53	**-0.10**	-0.69
	RMSE	1.84	1.67	**1.48**	1.52	1.50	1.56
	r	0.11	0.29	**0.53**	0.48	0.49	0.50
	IOA	0.42	0.46	0.65	0.62	**0.68**	0.58
October	Bias	-0.22	-0.70	-0.46	-0.42	**-0.06**	-0.73
	RMSE	2.02	1.85	**1.53**	1.70	1.58	1.66
	r	0.10	0.30	**0.56**	0.37	0.47	0.55
	IOA	0.44	0.51	**0.66**	0.54	0.65	0.60
November	Bias	**-0.23**	-0.83	-0.47	-0.41	-0.26	-0.77
	RMSE	1.98	1.88	**1.48**	1.68	1.56	1.61
	r	0.36	0.47	**0.66**	0.52	0.59	**0.66**
	IOA	0.60	0.62	**0.77**	0.68	0.75	0.70
December	Bias	-0.36	-1.22	-0.50	-0.34	**-0.08**	-0.80
	RMSE	2.01	2.28	**1.43**	1.54	1.46	1.59
	r	0.26	0.24	**0.66**	0.55	0.59	**0.66**
	IOA	0.53	0.51	**0.75**	0.68	0.74	0.67

To analyze wind direction, comparisons of WS10 and WD10 are made through joint frequency distribution plots, referred to as wind roses. In the present study, wind roses are displayed for the simulations which present the best statistical metrics, showing in Table 5, during wet and dry periods; they are compared with observations in Figures 4 and 5, respectively. As one can see, during wet period, MYJ and UW are the simulations that present the best statistics, whereas during dry period the best are MYJ and MYNN.

Table 5. Statistics of the comparison between observed and simulated WD10 data.

Month	Statistics	BouLac	GBM	MYJ	MYNN	UW	YSU
April	Bias	-19.62	-18.04	-13.92	-19.93	**-13.57**	-20.25
	RMSE	52.42	51.89	**49.98**	53.82	58.34	52.50
	r	0.31	0.34	**0.39**	0.22	0.30	0.32
May	Bias	-23.71	-20.54	-16.43	-26.68	**-16.03**	-24.87
	RMSE	75.45	74.95	**71.57**	76.80	76.37	74.44
	r	0.23	0.26	**0.29**	0.16	0.27	0.26
June	Bias	-13.67	26.44	-7.18	-18.11	**-3.04**	-14.86
	RMSE	84.66	106.01	81.48	79.66	89.07	**79.09**
	r	0.22	0.14	0.28	0.28	0.24	**0.31**
July	Bias	-8.35	8.08	**-1.28**	-7.04	-2.21	-9.16
	RMSE	**62.47**	70.34	69.90	70.80	63.29	69.81
	r	0.27	0.27	0.09	0.11	**0.35**	0.09
September	Bias	-2.44	-3.88	1.58	**-1.18**	3.46	-5.20
	RMSE	44.78	45.47	46.00	**43.74**	59.76	44.65
	r	0.32	0.30	0.35	**0.40**	0.17	0.34
October	Bias	-3.87	-4.19	**-2.63**	-3.39	-5.63	-5.30
	RMSE	61.72	66.24	**61.64**	63.98	64.93	64.89
	r	0.18	0.03	**0.19**	0.04	0.06	0.01
November	Bias	-4.25	2.13	**-1.00**	-4.17	-5.23	-5.21
	RMSE	60.53	62.66	59.71	**56.30**	60.02	59.42
	r	0.27	**0.34**	0.31	0.33	0.28	0.24
December	Bias	-3.98	6.04	-3.15	-4.55	**-1.09**	-6.56
	RMSE	54.39	64.24	57.61	**52.30**	57.32	54.22
	r	0.26	0.25	0.16	0.26	**0.34**	0.20

From the wind rose diagrams it can be seen that wind speed is underestimated, but wind directions are simulated fairly well for both periods. Observed wind roses during wet season (Figure 4) reveal that in April, winds blow mostly from the east (E) and the southeast (SE). In May and June, beyond winds from E and SE, the winds also come from the south (S), while in July, the winds blow again mostly from the east (E) and the southeast (SE). MYJ and UW (Figure 4) show similar patterns, however UW wind speed magnitudes are in better accordance with observed data. Both simulations MYJ and UW do not capture well the winds from E in July.

During dry period (Figure 5), as can be observed from the observed wind roses, the winds remain predominantly from the east (E), with slight variation from the northeast (NE). Simulations MYJ and MYNN were able to capture well the wind direction and they show similar patterns, almost the same. However, in September, the model predicts mostly winds from SE, which does not occur when the observed wind rose is analyzed.

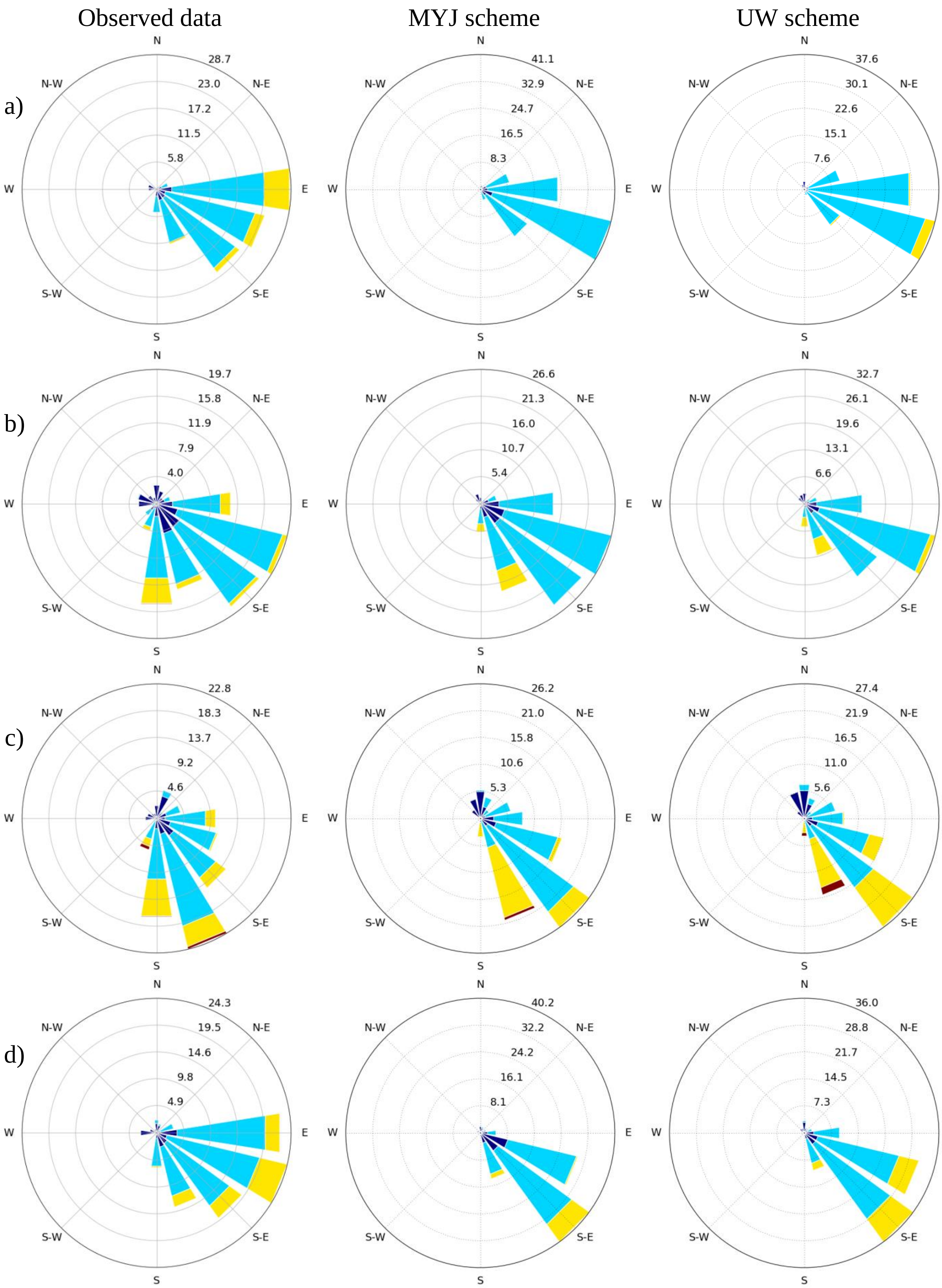

Figure 4: Comparison of wind roses obtained from MYJ and UW schemes with observations during wet period (AMJJ).

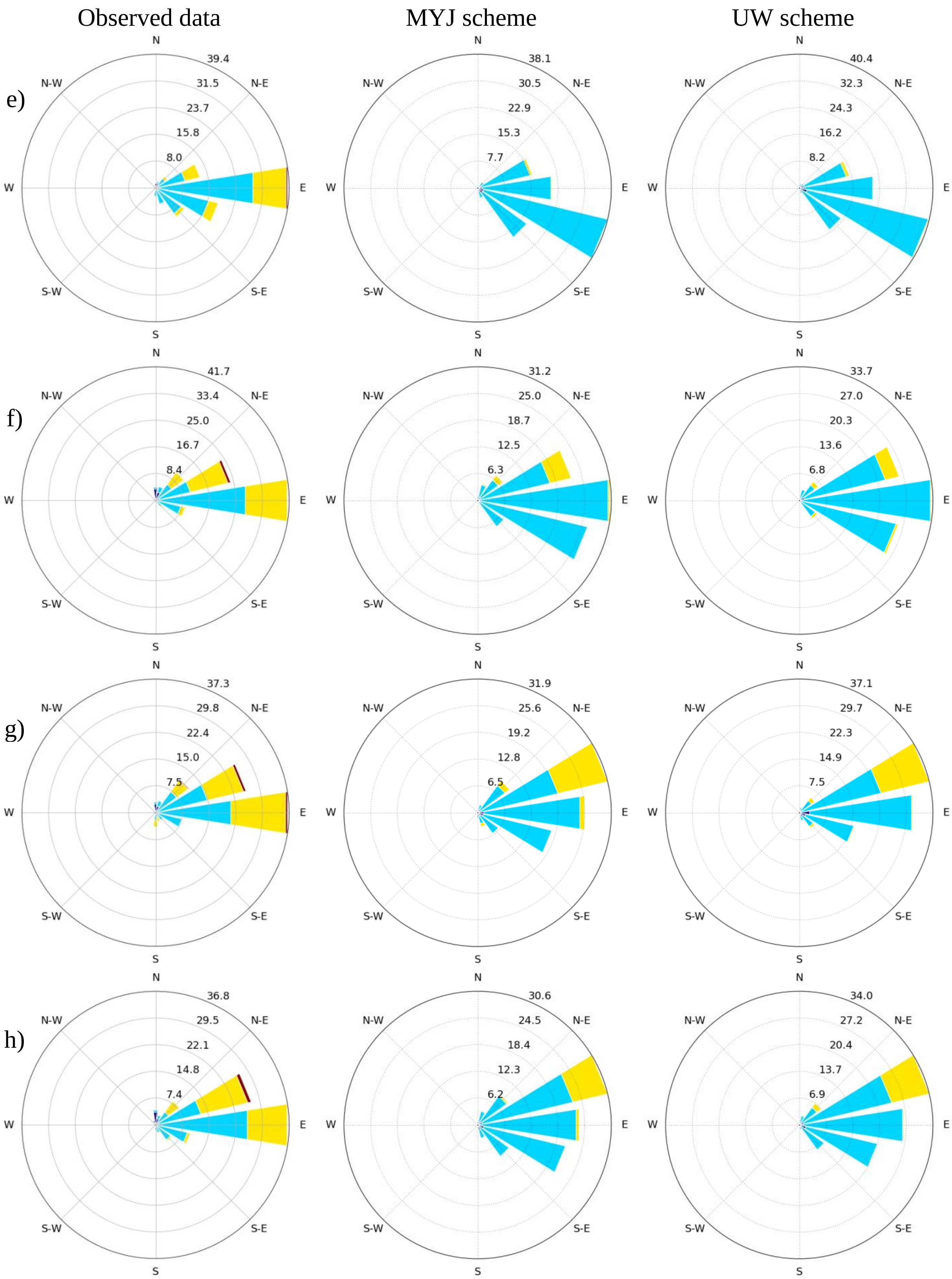

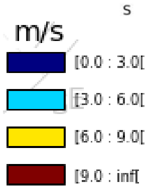

Figure 5: Comparison of wind roses obtained from MYJ and MYNN schemes with observations during dry period (SOND).

3.2 PBL height

Planetary boundary layer height (PBLH) was obtained from model using the six PBL schemes. Figure 7 shows comparison of mean diurnal variation of PBLH during wet and dry period. One could not compare simulated PBLH against observations, since observed PBLH measurements are not available. However it is worth mentioning that PBLH plays an important role in atmospheric numerical models since it is used for the estimation of mean quantities variables, and are also important for providing air pollution forecasts.

For each PBL scheme, there are different formulations of its estimation, leading to differences in their heights. For YSU, the PBLH is determined from bulk Richardson number by comparing with critical Richardson number (R_i=0 in convective boundary layer and 0<R_i<0.25 in stable boundary layer). In the case of BouLac, GBM, MYJ, MYNN and UW, PBLH is diagnosed as the height where prognostic TKE reaches a sufficiently small value (of the order of 0.005 m^2/s^2) (Shin & Hong, 2011).

Amongst all the schemes, from Figure 7, it is noticed that BouLac simulates highest (deepest) PBLH, and UW with GBM simulates (lowest) shallow PBLH for both periods. UW and GBM are similar, once UW is an improvement of GBM scheme, including cloud-top processes such as cloud-top cooling, evaporation, and phase change (Bretherton & Park, 2009).

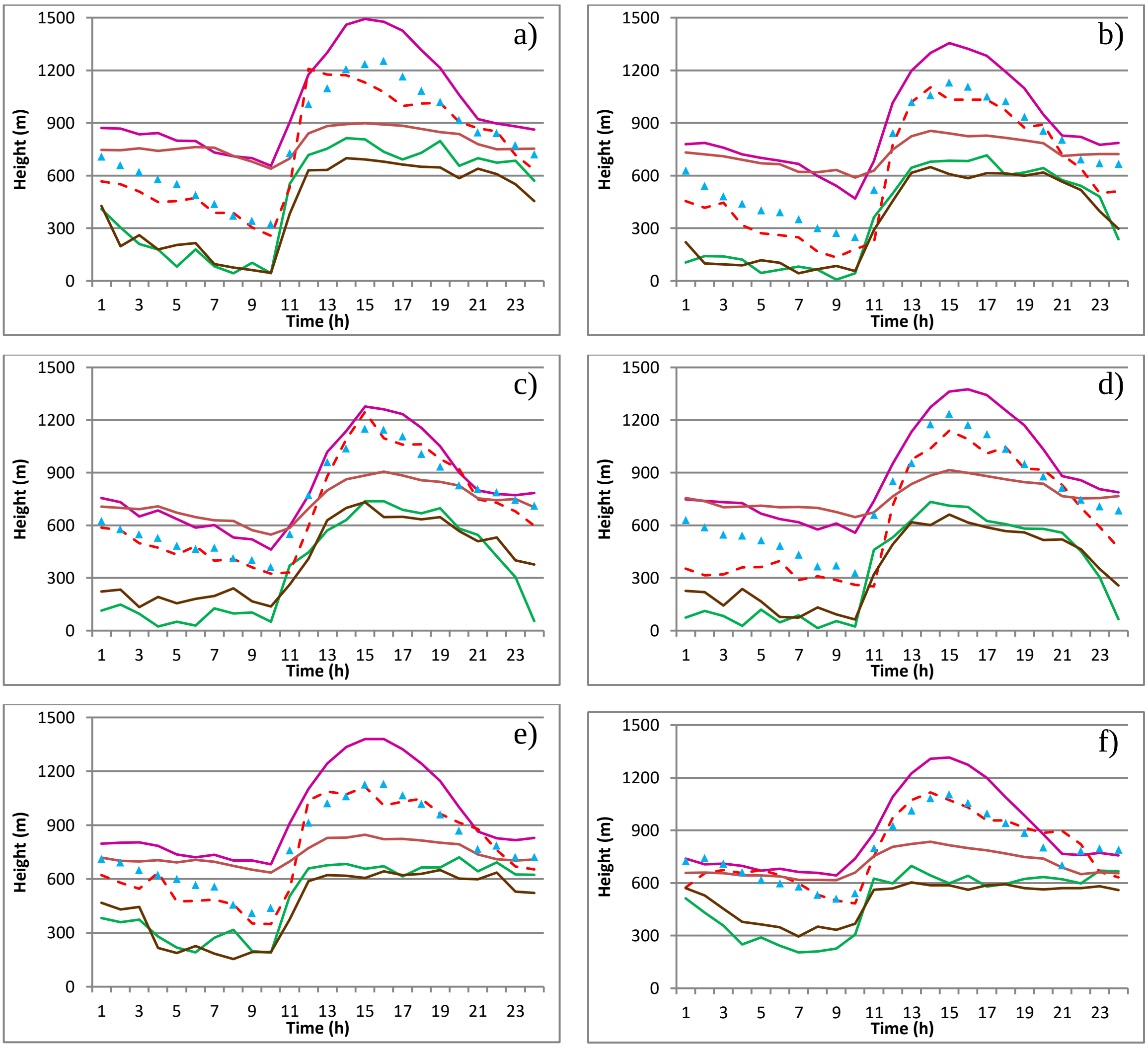

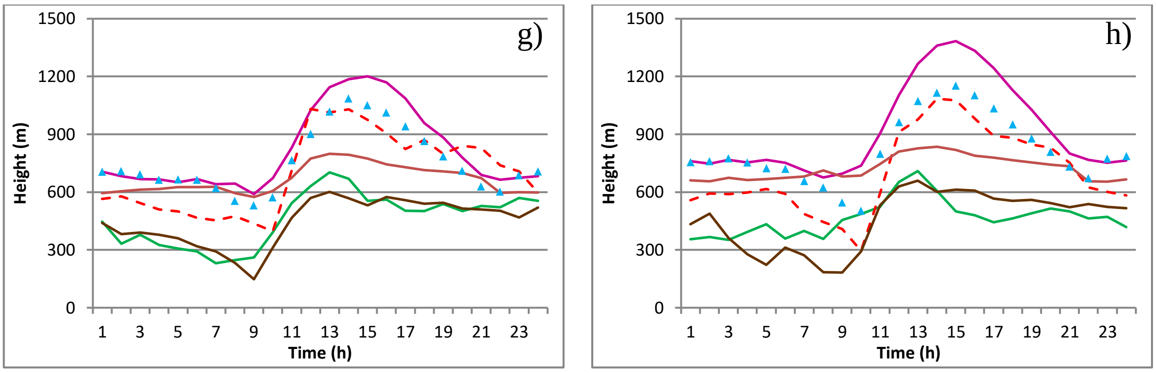

Figure 7: Time variation of the PBL in a) April and b) November at Airport station.

4 CONCLUSION

The main aim of the present study is to assess the performance of six PBL schemes (BouLac, GBM, MYJ, MYNN, UW and YSU) of the WRF-ARW model in simulating the surface meteorological parameters (T2, WS10 and WD10) and compared them with observations of the Airport station in the year of 2016 over the Metropolitan Region of Salvador (RMS). Simulations were performed for during wet (AMJJ) and dry (SOND) period in order to develop future works related to air pollution problems and eolic and solar energy in the region. After assessing all the meteorological parameters and periods, in general, MYJ scheme shows comparatively better performance. It is interesting to point out that local closures schemes, like MYJ, are suitable for stable conditions while non-local schemes are better suited for unstable atmospheric conditions. It would be worth looking into hybrid schemes (local and non-local models) since several studies has reported that they work well. Regardless of choice of PBL schemes, it is seen that model significantly underestimates the parameters. This work was a first step towards providing background to new studies about the local atmospheric circulation over RMS. It is evident that there is a need of a field measurement campaign in order to verify the results since some difficulties were faced due to the lack of meteorological information of the region.

Acknowledgements

The authors thank the Supercomputing Center for Industrial Innovation (Yemoja), the Fundação de Amparo à Pesquisa do Estado da Bahia (FAPESB) and also to the Coordenação de Aperfeiçoamento de Pessoal de Nível Superior (CAPES) for granting the master scholarship to the first author.

REFERENCES

Banks, R. F., Tiana-Alsina, J., Baldasano, J. M., Rocadenbosch, F., Papayannisd, A., Solomose, S., Tzanisf, C. G., 2016. Sensitivity of boundary-layer variables to PBL schemes in the WRF model based on surface meteorological observations, lidar, and radiosondes during the HygrA-CD campaign. *Atmospheric Research*, vol. 176-177, pp. 185-201. doi: 10.1016/j.atmosres.2016.02.024

Barreto, A. B., Aragão, M. R.S., Correia, M. F., Santos, A. H. M., 2008. Uma investigação sobre eventos intensos de chuva na cidade de Salvador, Bahia. In: *XV Congresso Brasileiro de Meteorologia (CBMET),* São Paulo.

Boadh, R., Satyanarayana, A. N. V., Rama Krishna, T. V. B. P. S., Madala, S., 2016. Sensitivity of PBL schemes of the WRF-ARW model in simulating the boundary layer flow parameters for their application to air pollution dispersion modeling over a tropical station. *Atmósfera*, vol. 29, pp. 61-81.

Bougeault, P., & Lacarrere P., 1989. Parameterization of orography-induced turbulence in a mesobeta-scale model. *Monthly Weather Review*, vol. 117, pp. 1872-1890. doi: 10.1175/1520-0493(1989)117<1872:POOITI >2.0.CO;2

Carvalho, D., Rocha, A., Gómez-Gesteira, M., Santos, C.S., 2014. Sensitivity of the WRF model wind simulation and wind energy production estimates to planetary boundary layer parameterizations for onshore and offshore areas in the Iberian Peninsula. *Applied Energy*, vol. 135, pp. 234–246.

Cohen, A. E., Cavallo, S. M., Coniglio, M. C., Brooks, H. E., 2015. A review of planetary boundary layer parameterization schemes and their sensitivity in simulating Southeastern U.S. cold season severe weather environments. *Weather and Forecasting*, vol. 30, pp. 591–612.

Dudhia, J., 1989. Numerical study of convection observed during the winter monsoon experiment using a mesoscale two-dimensional model. *Journal of the Atmospheric Sciences*, vol. 46, n. 20, pp. 3077–3107. doi: 10.1175/1520-0469(1989)046b3077:NSOCODN2.0.CO;2.

Grenier, H. & Bretherton C. S., 2001. A moist PBL parameterization for large-scale models and its application to subtropical cloud-topped marine boundary layers. *Monthly Weather Review*, vol. 129, pp. 357-377. doi: 10.1175/15200493(2001)129<0357:AMPPFL>2.0.CO;2

Gunwani, P. & Mohan, M., 2017. Sensitivity of WRF model estimates to various PBL parameterizations in different climatic zones over India. *Atmospheric Research*, vol. 194, pp. 43–65. doi: 10.1016/j.atmosres.2017.04.026

Hariprasad, K. B. R. R., Srinivas, C. V., Bagavath Singh, A., Vijaya Bhaskara Rao, S., Baskaran, R., Venkatraman, B., 2014. Numerical simulation and intercomparison of boundary layer structure with different PBL schemes in WRF using experimental observations at a tropical site. *Atmospheric Research*, vol. 145-146, pp. 27–44. doi: 10.1016/j.atmosres.2014. 03.023.

Hong, S.-Y., Dudhia, J., Chen, S.-H., 2004. A revised approach to ice microphysical processes for the bulk parameterization of clouds and precipitation. *Monthly Weather Review*, vol. 132, n. 1, pp. 103–120. doi: 10.1175/1520-0493(2004)132b0103:ARATIMN2.0.CO;2.

Hong, S.-Y., Noh., Y., Dudhia, J., 2006. A New Vertical Diffusion Package with an Explicit Treatment of Entrainment Processes. *Monthly Weather Review*, vol. 134, pp. 2318-2341. doi: 10.1175/MWR3199.1

Hu, X. M., Nielsen-Gammon, J. W., & Zhang, F., 2010. Evaluation of three planetary boundary layer schemes in the WRF model. *Journal of Applied Meteorology and Climatology*, vol. 49, n. 9, pp. 1831–1844. doi: 10.1175/2010JAMC2432.1.

Janjic, Z. I., 1994. The step-mountain eta coordinate model: further developments of the convection, viscous sublayer, and turbulence closure schemes *Monthly Weather Review*, vol. 122, pp. 927-945. doi: 10.1175/1520-0493(1994)122<0927:TSMECM>2.0.CO;2

Kain, J. S., 2004. The Kain–Fritsch convective parameterization: an update. *Journal of Applied Meteorology*, vol. 43, n. 1, pp. 170–181. doi: 10.1175/1520-450(2004)043b0170:TKCPAUN2.0.CO;2.

Mlawer, E. J., Taubman, S. J., Brown, P. D., Iacono, M. J., Clough, S. A., 1997. Radiative transfer for inhomogeneous atmospheres: RRTM, a validated correlated-k model for the longwave. *Journal of Geophysical Research*, vol. 102, pp. 16663-16682. doi: 10.1029/97JD00237.

Nakanishi, M. & Niino, H., 2006. An improved Mellor Yamada level-3 model: its numerical stability and application to a regional prediction of advection fog. *Boundary-Layer Meteorology*, vol. 119, pp. 397-407. doi: 10.1007/s10546-005-9030-8

Park, S. & Bretherton, C. S., 2009. The University of Washington shallow convection and moist turbulence schemes and their impact on climate simulations with the community atmosphere model. *Journal of Climate*, vol. 22, pp. 3449-3469. doi: 10.1175/2008JCLI2557.1

Queiroz, J. N., 2015. *Análise sinótica e multivariada de condições climáticas extremas na cidade de Salvador*. Dissertation, Federal University of Campina Grande/Campina Grande.

Rao, V. B.; Lima, M. C.; Franchito, S. H., 1993. Seasonal and interannual variations of rainfall over Eastern Northeast Brazil. *Journal of Climate*, vol. 6, pp. 1754-1763. doi: 10.1175/1520-0442(1993)006<1754:SAIVOR>2.0.CO;2

Salvador, N; Reis, N.C; Santos, J.M; Albuquerque, T.T.A; Loriato, A.G.; Delbarre, H.; Augustin, P.; Sokolov, A.; Moreira, D.M., 2016. Evaluation of weather research and forecasting model parameterizations under sea-breeze conditions in a North Sea coastal environment. *Journal of Meteorological Research*, vol. 30, pp. 998-1018.

Santos, A. P. P., 2013. Precipitação na cidade de Salvador: Classificação em quantis e análise de um evento climático extremo. Dissertation, Federal University of Campina Grande/Campina Grande.

Shin, H. H. & Hong, S.-Y., 2011. Intercomparison of Planetary Boundary-Layer Parametrizations in the WRF Model for a Single Day from CASES-99. *Boundary-Layer Meteorology*, vol. 139, pp. 261–281. doi: 10.1007/s10546-010-9583-z.

Silva, A. B., 2014. Análise em componentes principais das condições atmosféricas em episódios de rajadas de ventos na Região Metropolitana de Salvador. Dissertation, Federal University of Campina Grande/Campina Grande.

Skamarock, W. C., Klemp, J. B., Dudhia, J., Gill, D. O., Barker, D. M., Duda, M. G., Huang, X., Wang, W., Powers, J. G., 2008. *A Description of the Advanced Research WRF Version 3*. National Center for Atmospheric Research/Boulder, Colorado, USA.

Stull, R. B., 1988. *An Introduction to Boundary Layer Meteorology*. Kluwer Academic Press, Dordrecht, The Netherlands.

Surussavadee, C., 2017. Evaluation of WRF near-surface wind Simulations in Tropics Employing different planetary boundary layer schemes. *The 8th International Renewable Energy Congress (IREC 2017)*.

Yang, B., Qian, Y., Berg, L.K., Ma, P., Wharton, S., Bulaevskaya, V., Yan, H., Hou, Z., Shaw, W. J., 2016. Sensitivity of turbine-height wind speeds to parameters in planetary boundary-layer and surface-layer schemes in the Weather Research and Forecasting model. *Boundary-Layer Meteorology*, vol. 162, pp. 117–142. doi: 10.1007/s10546-016-0185-2.

Xie, B., Fung, J. C. H., Chan, A., & Lau, A., 2012. Evaluation of nonlocal and local planetary boundary layer schemes in the WRF model. *Journal of Geophysical Research*, vol. 117, D12103. doi:10.1029/2011JD017080)